====== **SOLID STATE** ======

Magnetic Braking and Energy Loss in Contactless Bearings Based on Superconducting Tapes

A. I. Podlivaev[a] and I. A. Rudnev[a],*

[a] National Research Nuclear University MEPhI (Moscow Engineering Physics Institute), Moscow, 115409 Russia
*e-mail: iarudnev@mephi.ru

Abstract—We consider magnetic braking and energy loss appearing in contactless bearings based on high-temperature superconducting tapes. We analyze model configurations of bearings in which a superconducting tape is the stator, while the rotor is a set of permanent magnets. It is shown that magnetic friction can be ignored in the case when the number of permanent magnets in the rotor is greater than eight. This result indicates the possibility of designing scaled magnetic bearings for long-term energy storage systems (e.g., kinetic storage rings).

INTRODUCTION

The use of a superconductor/permanent magnet couple in contactless bearings is promising not only due to the absence of friction forces in such bearings. The absence of direct mechanical contact between moving parts makes it possible to effectively employ magnetic bearings in high-speed devices such as gyroscopes and analogous instruments (see, for example, [1]).

The manufacturing of a superconducting rotor (stator) from a bulk high-temperature superconductor (HTSC) is a complex technological problem. First, HTSC materials (YBCO perovskite in our case) are quite brittle. Second, a complex annealing regime ensuring uniform superconducting properties of the material is required. An alternative to a bulk superconductor can be a composite superconductor consisting of stacks of HTSC tapes [2]. We can also assume that short-circuited coils prepared from HTSC tapes [3] are analogs of the tape stack that can be used in various levitation devices. The use of HTSC tapes instead of bulk materials has several advantages. The technology of manufacturing a superconductor composite assembled from tapes and having an arbitrary shape is simpler. The superconducting characteristics of a stack of tapes are not inferior to those of a bulk material [4]. In addition, HTSC tapes have better mechanical properties as compared to bulk materials.

The manufacturing of a magnetic rotor is also a technological problem. The one-piece magnet of the required shape and size must ensure an axially symmetric magnetic field. As in the case with a superconductor, an alternative to a one-piece magnet can be a composite magnet. Such a magnet has the form of a mosaic consisting of a large number of small magnets. Each element of the mosaic is a uniformly magnetized ferromagnet with the shape of a right parallelepiped. A disadvantage of such a mosaic is the nonuniformity of the magnetic field, which is especially noticeable at the joints of adjacent elements. The magnetic field nonuniformity may induce the hysteretic magnetization reversal in the superconductor. The magnetization reversal of the superconductor is accompanied by energy dissipation (see, for example, review [5]) and, hence, the emergence of a friction force in the bearing. This study is devoted to theoretical investigation of the effect of magnetic field nonuniformity of a mosaic magnet on the friction force in the bearing in which monolayer and multilayer rings made of second-generation HTSC tapes are considered as a superconductor stator.

1. DESCRIPTION OF THE BEARING MODEL. GEOMETRY. BASIC EQUATIONS

The bearing considered here consists of a rotor and a stator. The division into "rotor" and "stator" is conditional. The rotation of the inner bearing shaft and the outer part about the stationary internal axis is possible. For definiteness, we will henceforth assume that the superconducting part of the bearing is the stationary stator, while the rotor is formed by a set of small permanent magnets. Such a choice is due to the fact that it is technically easier to cool the stationary superconductor. The possibility of cooling allows us to disregard the overheating of the superconductor (otherwise, thermodynamic instability may occur [6, 7]). Second, the massive magnetic rotor rotating about the inner superconductor axis is optimal in the design of a
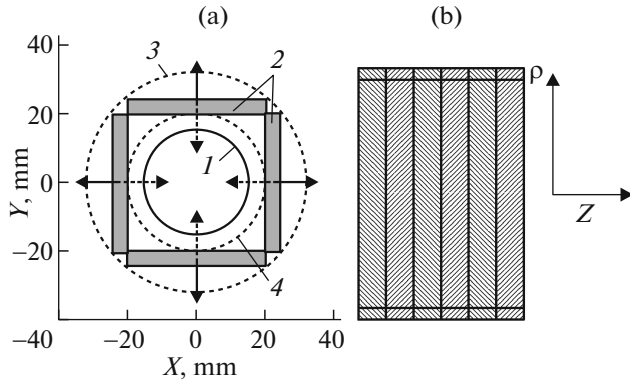
Fig. 1. Bearing with a tetragonal magnetic rotor. (a) End view: (*1*) superconducting stator; (*2*) magnetic rotor; (*3, 4*) outer and inner boundaries of the magnetic rotor (during its rotation), respectively. Solid and dashed arrows on the magnets show the direction of magnetization for adjacent (in the direction of the *Z* axis) magnets. (b) Magnetic rotor (six magnetic rings in the direction of the *Z* axis). Side view. Different hatchings indicate magnets with magnetic moments directed inwards and outwards relative to the rotor.

Fig. 2. Bearing with an octagonal magnetic rotor. End view: (*1*) superconducting stator; (*2*) magnetic rotor; (*3, 4*) outer and inner boundaries of the magnetic rotor (during its rotation), respectively.

gyroscope. Figures 1 and 2 show bearings with tetragonal and octagonal rotors, respectively. Henceforth, the number of magnets in the rotor will be denoted by N_{mag} ($N_{mag} = 4, 8, 16$). For calculations, we chose the following sizes of the magnetic rotor. The inner boundary of the rotor (internal dashed circle in Figs. 1 and 2) has a radius of 20 mm for the tetragonal as well as octagonal and dioctagonal rotors. The outer rotor boundary (external dashed circle in Figs. 1 and 2) has radii of 32.016 and 26.34 mm for the octagonal and dioctagonal rotors, respectively. For all rotors, the magnets have the same thickness of 5 mm (Figs. 1a and 2) and width $d_Z = 12$ mm in the direction of the *Z* axis (Fig. 1b). While choosing the tape parameters, we were oriented to a 12-mm SuperOx tape promising for applications (e.g., in current limiters [8]). The magnetization of each magnet is assumed to be uniform. If we denote by **m(r')** the magnetic moment density vector at a spatial point with radius vector **r'**, the magnetic induction vector produced by the magnet (occupying volume *V*) at point **r** has form [9]

$$\mathbf{B}(\mathbf{r}) = \mu_0 \int_V \left[\frac{3\mathbf{n}(\mathbf{n}, \mathbf{m}(\mathbf{r}')) - \mathbf{m}(\mathbf{r}')}{|\mathbf{r} - \mathbf{r}'|^3} \right] d^2 r', \tag{1}$$
$$\mathbf{n} = (\mathbf{r} - \mathbf{r}')/|\mathbf{r} - \mathbf{r}'|.$$

The modulus of vector **m(r')** was chosen so that the magnetic induction of the field produced by an individual magnet (see Fig. 1) at the center of its surface is 0.3 T.

The conventional thickness of an HTSC tape is about 0.1 mm; for this reason, like in [4], we assume that the thickness of the stator winding is zero. We also assume that the critical current density is j_c in a mono-
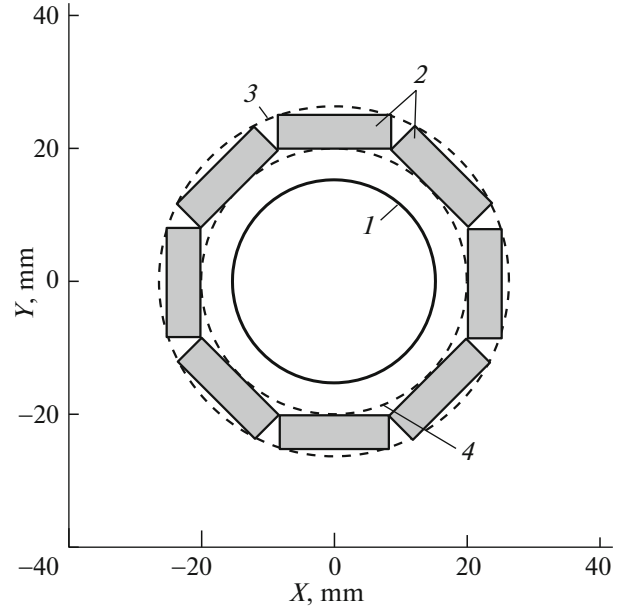
layer solid HTSC ring and $2j_c$ in a bilayer ring. The critical current density at the boundaries of adjacent rings perpendicular to the *Z* axis is zero. The *Z* coordinates of the stator ring boundaries coincide with the boundaries of heteropolar magnets of the rotor. These boundaries have coordinates $Z = 0, \pm d_Z/2, \pm 2d_Z/2, \pm 3d_Z/2, \pm 4d_Z/2$, etc.

For a large number of magnets in the rotor ($N_{mag} \gg 1$) and a small thickness of HTSC rings as compared to their perimeter ($d_p/d_Z \gg 1$), we can disregard the curvature of the stator and consider instead of the problem of determining the superconducting current density formulated in cylindrical coordinates (ρ, ϕ, *Z*) for ρ = R_S the two-dimensional problem in the (*p, Z*) plane, $p = R_S \phi$. The domain of definition of the magnetic field and current density in this case is rectangle $-d_Z/2 \le Z \le d_Z/2, -d_p/2 \le p \le d_p/2$. The boundary conditions are periodic in angular variable *p* as well as in variable *Z* (we assume that the rotor consists of an infinitely large number of contacting rings of heteropolar magnets). The replacement of the cylindrical problem by the planar problem is substantiated by the fact that, first, ratio $d_p/d_Z = 8$ is quite large; second, rotors with a large number of magnets ($N_{mag} = 8$ and 16) are most interesting for applications. We consider a tetragonal rotor for determining the qualitative dependence of the friction force in the bearing on the number of magnets. In addition, the effect of external field nonuniformity (in the angular variable) on the superconducting current distribution is manifested most precisely for the tetragonal rotor.

The external magnetic field produced by the magnetic rotor in the stator was calculated by formula (1). The magnetic field component normal to the stator surface is shown in Fig. 3 on this surface. The magnetic induction was determined for the tetragonal rotor.

Magnetic field amplitude variation $(B_{max} - B_{min})/(B_{max} + B_{min})$ for coordinate $Z = 0$ was 14.8%, 1.3%, and 0.2% for $N_{mag} = 4$, 8, and 16, respectively. The idea of using a nonuniform (periodic) external magnetic field is not novel. For example, in [10, 11], a set of heteropolar magnets was used for obtaining a periodic configuration; however, a distinguishing feature of our present study is the analysis of an HTSC tape in a weakly varying field that is acting, however, on the superconductor during an unlimited number of periods.

We describe the field dependence of the critical current in the superconducting tape using the two-exponential model [12] in which surface current density $j_c(B)$ of the HTSC tape has form

$$j_c(B) = A_1 \exp(-|B|/\beta_1) + A_2 \exp(-|B|/\beta_2) \quad (2)$$

with parameters $A_1 = 12.9$ kA/m, $A_2 = 13.8$ kA/m, $\beta_1 = 0.08$ T, and $\beta_2 = 1.92$ T. The spatial grid pitch in our calculations was $\delta h \sim 0.375$ mm. The calculation was based on the model of the critical state of the superconductor, which was initially proposed in [13]; some modifications and applications of this model were given in review [4]. Detailed descriptions of the formulation of the analytic problem and the numerical algorithm for field dependence (2) were given in [4, 14] and are not given here because of their cumbersome form.

The regime of variation of the external magnetic field was as follows. At the first stage, the magnetic field proportional to the field of the stationary rotor was increased monotonically from zero to the value determined by expression (1). Then, the rotor was rotated by 40 revolutions (the number of revolutions will be denoted by N_{rot}). We determined the corresponding density of superconducting currents. One turn of the cylindrical configuration corresponds to a magnetic field shift in the planar problem in variable p by period d_p. For this shift, the tangential component of the force of interaction of rotor field B_ρ with the currents of the stator (friction force) f_p for one stator ring was determined from Ampere law

$$f_p = \int_{-d_p/2}^{d_p/2} dp \int_{-d_Z/2}^{d_Z/2} B_\rho(p, Z) j_Z(p, Z) dZ. \quad (3)$$

2. RESULTS

The dependence of the friction force on the number of revolutions of the rotor for a tetragonal stator ($N_{mag} = 4$) is shown in Fig. 4. It can be seen that the
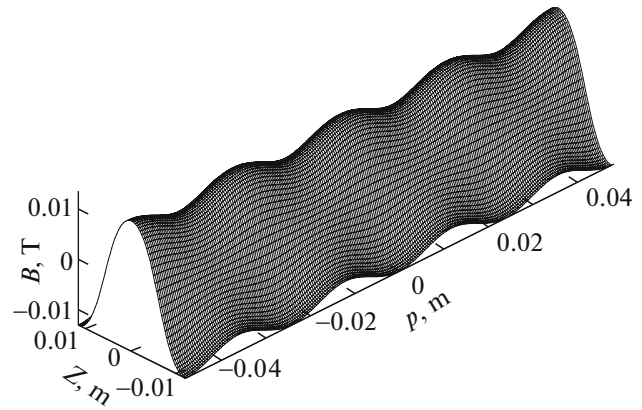

Fig. 3. Normal component of magnetic induction B_ρ on the developed surface of the stator.

friction force stabilizes after one turn. For rotors with larger numbers of magnets ($N_{mag} = 8$ and 16), this force stabilizes sooner than after two revolutions. In this study, we do not consider transient processes. For this reason, we determine the friction force by averaging this quantity from the third to the tenth revolution. In the case of the tetragonal rotor ($N_{mag} = 4$), the friction force for the monolayer/bilayer stator is 0.013 and 0.0021 N, respectively. In the case of the octagonal stator ($N_{mag} = 8$), the friction force for the monolayer/bilayer stator is 2.01×10^{-6} and 1.25×10^{-6} N, respectively. For $N_{mag} = 16$, the friction force for the monolayer/bilayer stator is 1.5×10^{-7} and 8.1×10^{-8} N, respectively.

The characteristic distributions of the superconducting current density in the stator and of the magnetic field for a tetragonal rotor are shown in Fig. 5. The upper part of the figure shows the superconducting current lines, while the lower part depicts the magnetic field lines of the rotor. The figure shows a fragment of the stator of width $2d_Z$ (the central tape is surrounded from top and bottom by halves of the neighboring tapes of the stator). During rotation of the rotor, the pattern is displaced periodically along the p axis.

For a qualitative interpretation of the dependence of the friction force on the number of magnets in the rotor, it is convenient to represent the stator by a system of interconnected magnetic pumps. Let us represent each mesh of the computational grid of size $h \times h$ on the stator as an elementary magnetic pump. If we denote by symbol ω the rotational frequency of the rotor, the frequency of pumping of each pump by an external varying magnetic field will be ωN_{mag} (the phases of field oscillations for meshes with different coordinates p will be different). The magnetic moment of the mesh induced by the external field is $g\mathbf{n}_\rho h^2$. Here, $\mathbf{n}_\rho$ is the unit vector of the normal to the stator surface. Quantity g is the magnetic moment density
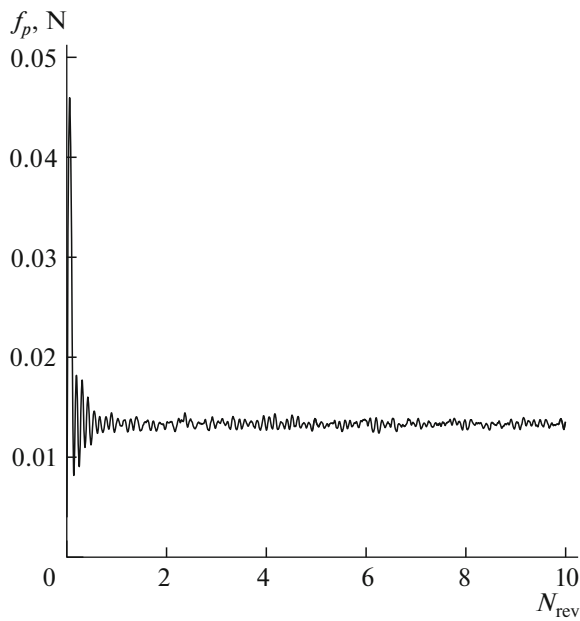
Fig. 4. Dependence of the friction force on the number of revolutions of the tetragonal rotor.

Fig. 5. Superconducting current lines (upper part) and level lines of the magnetic field component normal to the stator surface (lower part). A current line in the upper figure corresponds to a current of 5 A. A current line in the lower figure corresponds to a magnetic induction of 0.02 T.

connected with the surface current density $\mathbf{j}(p, Z)$ of the stator by relation $\mathbf{j}(p, Z) = \nabla(g\mathbf{n}_\rho)$ (see review [5] and the literature sited therein). Figure 6 shows the dependence of the magnetic moment density of a mesh with coordinates $p = 0$, $Z = 0$ on the magnetic induction of the rotor at this point. The upper and lower curves correspond to monolayer and bilayer HTSC stators, respectively. The curves are shown for one revolution of the rotor after the termination of transient processes. The magnetic induction at the given point varies from minimal value $B_{\min} = 0.095$ T to maximal value $B_{\max} = 0.128$ T.

On the segment of the curve corresponding to the magnetic induction increasing from minimal $B_{\min}$ to maximal $B_{\max}$ value, the emf of the varying field induces currents reducing the magnetic moment density (the induced magnetic field is opposite to the inducing field). Therefore, the magnetic moment is minimal for the maximal magnetic field. The screening process is limited by the critical current (otherwise, the screening would be complete in the entire stator). Upon a decrease of the magnetic field from the maximal value at the initial stage, the emf changes its sign, and the current density at this point passes through zero, and then its value attains the critical current density. The amplitude of the magnetic induction variation for a tetragonal rotor on the stator surface reaches 14.8% of the mean value. This variation is sufficient for, first, the sign reversal of the magnetic moment of a mesh in the monolayer stator (upper curve in Fig. 6), the magnetic field polarity remaining unchanged. Second, due to the smallness of the critical current for such a field variation, the stator experi-
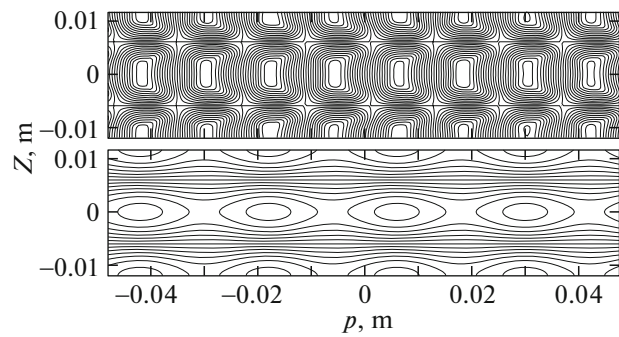
ences radical magnetization reversal, which leads to a wide hysteresis loop (and as a consequence, to energy dissipation and large friction force). Doubling of the critical current density in the bilayer stator blocks the magnetization reversal process (lower curve in Fig. 6). The hysteresis loop area sharply decreases and, as a consequence, the friction force decreases also. The substantial decrease in the friction force upon an increase in the number of magnets is explained analogously. The variation of the magnetic field amplitude by 1.3 and 0.2% for $N_{\text{mag}} = 8$ and 16 is insufficient for the magnetization reversal of even a monolayer stator.
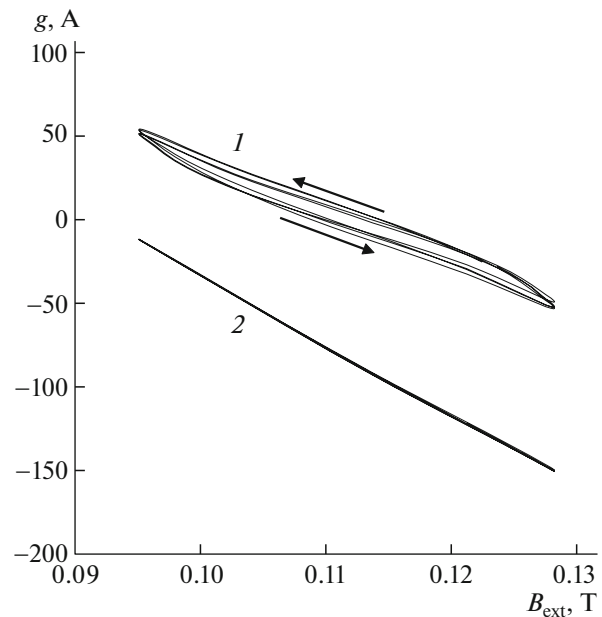

Fig. 6. Dependence of the magnetic moment density at the point with coordinates $p = 0$, $Z = 0$ on the magnetic induction for a single revolution of the rotor: (*1*) dependence for a monolayer stator; (*2*) dependence of the bilayer stator. Arrows indicate the direction of path tracing of the hysteresis loop during rotor rotation.

CONCLUSIONS

Our calculations have shown that the magnetic friction force and energy loss associated with it do not prevent designing a composite bearing in which the rotor consists of more than eight magnets and the stator consists of several short-circuited layers of second-generation HTSC tapes. Experimental verification of this conclusion and analysis of the effect of other bearing parameters (eccentric position and skewing of the rotor axis relative to the stator axis, defects in the HTSC tape of the stator, and so on), which can critically deteriorate its characteristics, will be performed separately.

It should be noted that the configuration of the magnetic rotor and the superconducting stator made of HTSC tapes is basically advantageous as compared to bearings based on bulk HTSC parts because it permits almost unlimited scaling of the device.

FUNDING

CONFLICT OF INTEREST

The authors claim that there is no conflict of interest.

REFERENCES

1. Y. Miyazaki, K. Mizuno, T. Yamashita, M. Ogata, H. Hasegawa, K. Nagashima, S. Mukoyama, T. Matsuoka, K. Nakao, S. Horiuch, T. Maeda, and H. Shimizu, Cryogenics **80**, 234 (2016).

2. K. Liu, W. Yang, G. Ma, L. Quéval, T. Gong, C. Ye, X. Li, and Z. Luo, Supercond. Sci. Technol. **31**, 015013 (2018).

3. M. V. Kozintseva, A. M. Bishaev, A. A. Bush, M. B. Gavrikov, K. E. Kamentsev, N. A. Nizhel'skii, V. V. Savel'ev, and A. S. Sigov, Tech. Phys. **62**, 890 (2017).

4. I. A. Rudnev and A. I. Podlivaev, IEEE Trans. Appl. Supercond. **26**, 8200104 (2016).

5. Ch. Jooss, J. Albrecht, H. Kuhn, S. Leonhardt, and H. Kronmuller, Rep. Prog. Phys. **65**, 651 (2002).

6. V. R. Romanovskii, Tech. Phys. **62**, 58 (2017).

7. V. R. Romanovskii, Tech. Phys. **62**, 560 (2017).

8. D. F. Alferov, M. R. Akhmetgareev, D. V. Evsin, I. F. Voloshin, A. V. Kalinov, L. M. Fisher, and E. V. Tskhai, Tech. Phys. **63**, 26 (2018).

9. L. D. Landau and E. M. Lifshitz, *Field Theory* (Nauka, Moscow, 1988).

10. B. A. Bazarov, V. F. Ezhov, N. A. Kovrizhnykh, V. L. Ryabov, A. Z. Andreev, A. G. Glushkov, V. A. Knyaz'kov, and G. B. Krygin, Tech. Phys. Lett. **42**, 663 (2016).

11. A. I. Podlivaev, S. V. Pokrovskii, I. V. Anishchenko, and I. A. Rudnev, Tech. Phys. Lett. **43**, 1136 (2017).

12. A. I. Podlivaev, I. A. Rudnev, and N. P. Shabanova, Bull. Lebedev Phys. Inst. **41**, 351 (2014).

13. C. P. Bean, Phys. Rev. Lett. **8**, 250 (1962).

14. A. Podlivaev and I. Rudnev, Supercond. Sci. Technol. **30**, 035021 (2017).

Translated by N. Wadhwa